






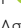


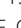





α -Synuclein phosphorylation at serine 129 occurs after initial protein deposition and inhibits seeded fibril formation and toxicity

Simona S. Ghanem^{a,1}, Nour K. Majbour^{a,1}, Nishant N. Vaikath^{a,1} , Mustafa T. Ardah^b, Daniel Erskine^c, Nanna Møller Jensen^{d,e} , Muneera Fayyad^a, Indulekha P. Sudhakaran^a , Eftychia Vasili^f , Katerina Melachroinou^g , Ilham Y. Abdi^a , Ilaria Poggiolini^a, Patricia Santos^f , Anton Dorn^h , Paolo Carloni^{i,j,k} , Kostas Vekrellis^g, Johannes Attems^c , Ian McKeith^c , Tiago F. Outeiro^{l,m}, Poul Henning Jensen^{d,e} , and Omar M. A. El-Agnaf^{a,2}

Edited by Anders Björklund, Lund University, Lund, Sweden; received June 3, 2021; accepted February 15, 2022

α -Synuclein (α -syn) phosphorylation at serine 129 (pS129- α -syn) is substantially increased in Lewy body disease, such as Parkinson's disease (PD) and dementia with Lewy bodies (DLB). However, the pathogenic relevance of pS129- α -syn remains controversial, so we sought to identify when pS129 modification occurs during α -syn aggregation and its role in initiation, progression and cellular toxicity of disease. Using diverse aggregation assays, including real-time quaking-induced conversion (RT-QuIC) on brain homogenates from PD and DLB cases, we demonstrated that pS129- α -syn inhibits α -syn fibril formation and seeded aggregation. We also identified lower seeding propensity of pS129- α -syn in cultured cells and correspondingly attenuated cellular toxicity. To build upon these findings, we developed a monoclonal antibody (4B1) specifically recognizing nonphosphorylated S129- α -syn (WT- α -syn) and noted that S129 residue is more efficiently phosphorylated when the protein is aggregated. Using this antibody, we characterized the time-course of α -syn phosphorylation in organotypic mouse hippocampal cultures and mice injected with α -syn preformed fibrils, and we observed aggregation of nonphosphorylated α -syn followed by later pS129- α -syn. Furthermore, in postmortem brain tissue from PD and DLB patients, we observed an inverse relationship between relative abundance of nonphosphorylated α -syn and disease duration. These findings suggest that pS129- α -syn occurs subsequent to initial protein aggregation and apparently inhibits further aggregation. This could possibly imply a potential protective role for pS129- α -syn, which has major implications for understanding the pathobiology of Lewy body disease and the continued use of reduced pS129- α -syn as a measure of efficacy in clinical trials.

Parkinson's disease | α -synuclein | phosphorylation

Parkinson's disease (PD) and dementia with Lewy bodies (DLB) are both associated with underlying Lewy body disease, which represents the second most common neurodegenerative disorder after Alzheimer's disease (1, 2). The neuropathological hallmark of Lewy body disease is the intracellular aggregation of the protein α -synuclein (α -syn) into spherical cytoplasmic inclusions, termed Lewy bodies, but are also observed in neuronal processes as Lewy neurites (LNs) (3).

α -Syn is thought to play a central role in the pathobiology of Lewy body disease. Single-point mutations and genetic modifications affecting α -syn expression—through duplications, triplications, or polymorphisms in its promoter—have been linked to both idiopathic and familial forms of Lewy body disease (4–6). Nevertheless, neuropathological studies utilizing pan- α -syn antibodies, recognizing both physiological and pathological forms of the protein, do not consistently report a relationship between the load of Lewy body pathology and clinical disease severity (2). To reconcile the apparent importance of α -syn in Lewy body disease with the difficulty relating Lewy body burdens in the brain to phenotypic severity, continued research has focused on the identification of particularly disease-relevant forms of α -syn. α -Syn undergoes various posttranslational modifications (PTMs)—including acetylation, nitration, ubiquitination, and glycosylation and phosphorylation at serine 129 (pS129)—increases from ~4% under physiological conditions to 90% in Lewy body disease, suggesting it is associated with the disease state (7–9).

Previous studies have reported that pS129 enhances intracellular aggregate formation in SH-SY5Y cells (10), and mediates cell death through activation of the unfolded protein response pathway (11). Furthermore, studies in rodent models have suggested that pS129 exacerbates the rate of pathological protein aggregation and deposition, with subsequent negative effects on neuronal functioning (12). However, these studies are

Significance

Converging evidence points to the build-up of phosphorylated α -synuclein (α -syn) at residue serine 129 (pS129) in Lewy body disease, suggesting its central role in the regulation of α -syn aggregation and neuronal degeneration. However, a comprehensive understanding of the role of α -syn phosphorylation at pS129 in α -synucleinopathies pathogenesis is still lacking. Herein, we study the phosphorylation incidence and its effect on α -syn aggregation propensity and cellular toxicity. Collectively, our data suggest that pS129 occurred subsequent to initial α -syn aggregation, lessened aggregation propensity, and attenuated cytotoxicity through diverse assays. Our findings highlight major implications for a better understanding of the role of a molecular modification on protein aggregation.

Author contributions: T.F.O., P.H.J., and O.M.A.E.-A. designed research; S.S.G., N.K.M., N.N.V., M.T.A., D.E., N.M.J., M.F., I.P.S., E.V., K.M., I.Y.A., I.P., P.S., A.D., and P.C. performed research; S.S.G., N.K.M., N.N.V., N.M.J., K.V., J.A., and I.M. analyzed data; K.V., J.A., I.M., T.F.O., P.H.J., and O.M.A.E.-A. contributed to data interpretation; S.S.G. wrote the paper; D.E., K.V., J.A., I.M., T.F.O., P.H.J., and O.M.A.E.-A. contributed to critical revision; and O.M.A.E.-A. provided final approval.

The authors declare no competing interest.

This article is a PNAS Direct Submission.

Copyright © 2022 the Author(s). Published by PNAS. This open access article is distributed under Creative Commons Attribution-NonCommercial-NoDerivatives License 4.0 (CC BY-NC-ND).

¹S.S.G., N.K.M., and N.N.V. contributed equally to this work.

²To whom correspondence may be addressed. Email: oelagnaf@hbku.edu.qa.

This article contains supporting information online at <http://www.pnas.org/lookup/suppl/doi:10.1073/pnas.2109617119/-DCSupplemental>.

Published March 30, 2022.

counterbalanced by others reporting a potentially neuroprotective function of phosphorylation in animal models (13, 14) and cellular model systems (15). Additionally, studies have reported neutral findings regarding pS129 modification as neither enhancing nor diminishing cellular toxicity and α -syn aggregation (16, 17). Despite the uncertain pathogenic role of pS129 in Lewy body disease, antibodies against pS129 are widely used, based on the putative view that they label a species of α -syn that is particularly disease-relevant. These studies often employ pS129- α -syn as a marker of the abundance of protein inclusions to stage disease severity and evaluate the relationship between its abundance and important clinical or pathological variables, such as disease duration, phenotypic severity, or cell loss (18). Such studies typically identify that pS129 abundance throughout the brain correlates with disease severity (19–21), though it remains uncertain whether phosphorylation precedes protein aggregation or occurs secondarily to deposition of non-phosphorylated α -syn, and whether pS129 is a key driver of pathogenicity or simply a useful marker of a neurodegenerative process (22, 23). Therefore, although there is a substantial literature on pS129 in Lewy body disease, there is continued controversy regarding its potential contribution to disease states, with numerous studies reporting discordant findings. Despite contradictory findings regarding the disease-relevance of pS129, it is widely viewed as a particularly disease-associated modification, thus necessitating further research to address its importance for Lewy body disease.

To address the key questions regarding the pathogenic relevance of pS129- α -syn, the present study aimed to undertake a comprehensive and multidisciplinary project to address this important and pressing question. The key aim of the study was to better understand the role of pS129 in the natural history of Lewy body disease, by determining when pS129 occurs in the development of α -syn aggregates and how it affects the aggregation-propensity and cytotoxicity of α -syn

Results

pS129 Inhibits α -syn Aggregation. As pS129- α -syn is most abundant under disease conditions, we evaluated the effect of pS129 on α -syn aggregation to determine whether this modification influences the rate at which α -syn aggregates. Pure monomeric α -syn was mixed with different concentrations of pS129- α -syn (0 to 100%), incubated for up to 20 d, and Thioflavin-S (Th-S) binding assay showed the aggregation at various time points. As expected, the nonphosphorylated monomeric α -syn aggregated gradually reaching $\sim 35,000$ Th-S counts after 20 d of incubation (Fig. 1A). In accordance with previous studies (24), the sample containing 5% pS129- α -syn exhibited a similar aggregation trend to the nonphosphorylated sample (Fig. 1A). The sample with 20% of pS129- α -syn showed a significant decrease in aggregation, given that the reduction in Th-S fluorescence readings was more than 50%. Moreover, fibril formation in samples containing 50% and 100% of pS129- α -syn was almost completely inhibited, with Th-S fluorescence readings reaching $\sim 2,000$ counts after 20 d of incubation. Thus, these results indicate that phosphorylation at S129 exerts an inhibitory effect on α -syn aggregation.

pS129 Has Reduced Ability to Seed the Aggregation of α -syn.

The inhibitory effect of pS129- α -syn on α -syn aggregation prompted us to evaluate whether pS129- α -syn has an effect on seeded aggregation of α -syn. We generated phosphorylated monomeric and aggregated recombinant α -syn (*SI Appendix*,

Fig. 1 A and B) and confirmed phosphorylation of α -syn by immunoblotting using anti-pS129- α -syn antibody (*SI Appendix*, Fig. 1C). We also generated WT and pS129- α -syn pure fibrils and pure seeds (performed fibrils, PFFs) and characterized these with Th-S fluorescence and electron microscopy (*SI Appendix*, Fig. 1 D and E).

Addition of nonphosphorylated S129- α -syn (WT- α -syn) PFFs (2 μ M) to monomeric α -syn led to a dramatic increase in Th-S fluorescence, suggesting increased fibrillization, compared to monomeric α -syn alone (Fig. 1B). It is notable that, while WT PFFs led to α -syn aggregation at 0.1 μ M, the same concentration of pS129- α -syn PFFs did not induce aggregation (Fig. 1C). For pS129- α -syn to seed aggregation in this system, 2 μ M was required, but its rate of aggregation was still reduced compared to WT- α -syn PFFs (Fig. 1B).

To complement our findings regarding seeded aggregation of pS129- α -syn, we next asked whether seed-competent exogenous PFFs could induce the aggregation of pS129- α -syn monomer. However, we noted that pS129- α -syn monomers failed to aggregate even after 48 h of incubation after adding either WT- α -syn PFFs or pS129- α -syn PFFs. Taken together, these findings suggest that pS129- α -syn has an inhibitory effect on α -syn seeded aggregation (Fig. 1 D and E).

Inhibitory Seeding Effect of pS129- α -syn on Real-Time Quaking-Induced Conversion Assay Using Brain Homogenates from PD and DLB Cases and pS129- α -syn Impact on Aggregation Kinetics.

To further determine the ability of pS129- α -syn to aggregate, we employed the real-time quaking-induced conversion (RT-QuIC) assay of nucleation-dependent α -syn polymerization (25). To seed aggregation in this assay, we used brain tissue from temporal and frontal cortex samples of PD ($n = 4$) and DLB ($n = 4$) cases with neuropathological confirmation of Lewy body disease. To determine the ability of pS129- α -syn to aggregate, we used pS129- α -syn as substrate in the RT-QuIC assay and compared its aggregation capacity to WT- α -syn. In contrast to WT- α -syn, which demonstrated robust aggregation, pS129- α -syn showed reduced aggregation with a longer lag time, decreased amyloid formation rate, and shorter F_{MAX} (maximum intensity of fluorescence) (Fig. 2 A–G and Table 1). These data are consistent with pS129- α -syn having an inhibitory effect on α -syn aggregation.

It is noteworthy that pS129- α -syn phosphorylation buffer constituents, which include ATP and magnesium, did not affect the rate of α -syn aggregation (*SI Appendix*, Fig. 2A), its ability to seed α -syn aggregation (*SI Appendix*, Fig. 2B), and nucleation-dependent RT-QuIC assay (*SI Appendix*, Fig. 2C). It is interesting to note that Western blot analysis on TBS fractions of PD and DLB lysates failed to detect pS129- α -syn (*SI Appendix*, Fig. 3A). Additionally, immunodepletion of WT- α -syn by 4B1 (*SI Appendix*, Fig. 3 B and C) in DLB brain lysates demonstrated no evident of seeded aggregation as shown by RT-QuIC assay (*SI Appendix*, Fig. 3D).

Moreover, possible interactions between phosphorylated Ser-129 and other residues of α -syn and their effect on aggregation kinetics were identified by molecular simulations reported by a previous study (26). The conformer shown in Fig. 2H illustrates that phosphorylated serine at 129 might interact locally with Lys-96 and Lys-97 (dashed lines in Fig. 2H), stabilizing the loop between residues 96 and 129. In addition, it might form long-range electrostatic interactions with the N terminal (dotted line in Fig. 2H), which is highly positive, featuring as many as 11 lysine residues. These interactions may increase the

Table 1. RT-QuIC kinetic parameters of the relative seeding activity for monomeric- α -syn/pS129- α -syn in frontal and temporal regions extracted from PD and DLB cases

Seed	Substrate	Lag-phase \pm SD	Amyloid formation rate \pm SD (1/h)	F_{MAX} (RFU $\times 10^3$) \pm SD
PDfrontal	α -syn	26 \pm 3.4	0.04 \pm 0.005	180 \pm 57
	pS129- α -syn	94 \pm 45	0.013 \pm 0.008	69.8 \pm 58.7
PDtemporal	α -syn	19.8 \pm 2.5	0.05 \pm 0.006	199 \pm 34.8
	pS129- α -syn	104 \pm 34	0.01 \pm 0.003	32.2 \pm 5
DLBfrontal	α -syn	37.8 \pm 6	0.027 \pm 0.005	131 \pm 93
	pS129- α -syn	132 \pm 31	0.007 \pm 0.0019	27.7 \pm 4
DLBtemporal	α -syn	22.5 \pm 4	0.045 \pm 0.008	259 \pm 0.571
	pS129- α -syn	88 \pm 45	0.013 \pm 0.006	118 \pm 99

frequency of contacts between the C terminal and the N terminal, already observed in the unmodified protein (26).

Addition of pS129- α -syn Monomers to Preformed Aggregates in Cells Did Not Promote Seeding-Mediated Toxicity. We next sought to evaluate the effect of pS129- α -syn aggregation on cytotoxicity, as neurodegeneration is thought to be a key disease-relevant sequela of α -syn aggregation. We determined the cytotoxicity of pure PFFs (sonicated fibrils) and fibrils (nonsonicated) (2, 5, and 10 μ M) on BE (2)-M17 and SH-SY5Y WT cells in the presence or absence of WT- α -syn monomers. Both α -syn species affected cell viability in both BE (2)-M17 and SH-SY5Y cells at all tested concentrations, as shown in Fig. 3 *A* and *B*. Despite the fact that PFFs exhibited more toxicity than fibrils, adding monomeric WT- α -syn significantly exacerbated this effect (*SI Appendix, Fig. 4*) and knockdown of α -syn with small-interfering RNA (siRNA) significantly reduced this effect (*SI Appendix, Fig. 5*). Thus, monomeric α -syn is vital for fibril- and seed-mediated toxicity.

Given the critical importance of α -syn monomers in mediating the toxicity of fibrils and PFFs, we next asked whether pS129- α -syn monomers would also contribute enhanced cytotoxicity to BE (2)-M17 and SH-SY5Y WT cells. Monomeric pS129- α -syn employed at a range of concentrations (0.31 to 20 μ M) did not show toxicity in BE (2)-M17 cells (*SI Appendix, Fig. 6A*) and SH-SY5Y cells (*SI Appendix, Fig. 6B*). BE (2)-M17 and SH-SY5Y WT cells were treated with different concentrations of either pure fibrils or pure PFFs (2, 5, and 10 μ M) and after 1 h of incubation, monomeric pS129- α -syn was added to the cells at a final concentration of 10 μ M. As shown in Fig. 3 *C* and *D*, pS129 monomers had no effect on the viability of cells pretreated with various concentrations of pure fibrils or PFFs, with the toxicity levels observed comparable to the group treated only with pure PFFs or fibrils. Therefore, the addition of WT monomers enhances the cytotoxicity of PFFs and fibrils, but the pS129 modification abolishes this effect.

pS129- α -syn PFFs Are Less Potent in Seeding α -syn Aggregation in Cells. To further investigate the seeding efficiency of α -syn PFFs in vitro, we used a stable cell line overexpressing α -syn fused to EGFP (HEK293- α -syn-EGFP) under the cytomegalovirus promoter, to examine whether the exogenous addition of different α -syn PFFs affected the seeding of endogenous α -syn. We treated cells with either WT- α -syn PFFs or with pS129- α -syn PFFs at a final concentration of 100 nM and incubated for 4 d and compared to control cells exposed to vehicle only (PBS). Cells were then evaluated by microscopy and the percentage of cells with intracellular accumulation of α -syn-EGFP was counted. Interestingly, we found that the internalized WT- α -syn PFFs resulted in a significant increase

of the α -syn-EGFP inclusions compared to control cells (Fig. 4*A*). In contrast, exposure of cells to pS129- α -syn PFFs caused a significantly lower percentage of cells with α -syn inclusions when compared to the WT- α -syn-treated cells, but yet significantly higher than control cells (Fig. 4*B*).

Development and Validation of Specific Antibody against Nonphosphorylated α -syn at Serine 129. Following the hybridoma technology for monoclonal antibody development, a mouse monoclonal antibody specific for WT- α -syn was generated, named 4B1. The isotype was determined as IgG1 and the antibody was purified and thoroughly characterized. The specificity of 4B1 for recombinant WT-, pS129-, or mutated S129A- α -syn (with a substitution of serine 129 to alanine) proteins was assessed by Western blot and demonstrated that 4B1 is specific for WT- α -syn and did not recognize pS129- α -syn under these denaturing conditions (Fig. 5*A*). Furthermore, there was no evident band when serine was replaced with alanine (S129A- α -syn), indicating that S129 is an integral residue of the epitope recognized by 4B1 (Fig. 5*A*). Syn-1 (mouse anti- α -syn, BD Bioscience) and pS129 (in-house mouse anti pS129- α -syn antibody) (27) antibodies were included as controls (Fig. 5*A*). Given that monomeric α -syn undergoes different conformational changes forming oligomers and amyloid fibrils (28, 29), we further assessed the specificity of 4B1 antibody against different conformations of the protein. Surprisingly, after extensive non-denaturing characterization using filter retardation assay (Fig. 5 *B, i*), inhibition ELISA (Fig. 5 *B, ii*), and sandwich ELISA (Fig. 5 *B, iii*), we found that 4B1 preferentially recognizes β -sheet-rich structures (fibrils, ONE-, or HNE-oligomers) and did not recognize the monomeric form of WT- α -syn. This suggested that the epitope for 4B1 might be hidden in solution, and exposed under these denaturing conditions. In order to confirm this observation, we treated α -syn PFFs and fibrils with increasing concentrations of denaturing buffer containing either SDS or urea. The treated samples were subjected to a filter retardation assay using both 4B1 and syn-O2, which is specific for α -syn aggregates (27). Additionally, the generic 11D12 mouse monoclonal anti- α -syn antibody was used (27).

The results confirmed that 4B1 is specific toward α -syn aggregates (PFFs and fibrils), as compared to low detection of these samples after being treated with denaturing buffers (Fig. 5 *B, iv*). Additionally, filter retardation assay analysis showed that 4B1 specifically recognized WT- α -syn fibrils and did not label β - or γ -syn fibrils (Fig. 5 *B, v*). F11 (mouse monoclonal anti- $\alpha/\beta/\gamma$ synuclein antibody, Santa Cruz Biotechnology), E-20 (mouse monoclonal anti- γ -syn antibody, Santa Cruz Biotechnology) were included as control antibodies. Additionally, 4B1 recognized both human and mouse WT- α -syn fibrils to an equal extent (Fig. 5 *B, v*). Immunofluorescence analysis on

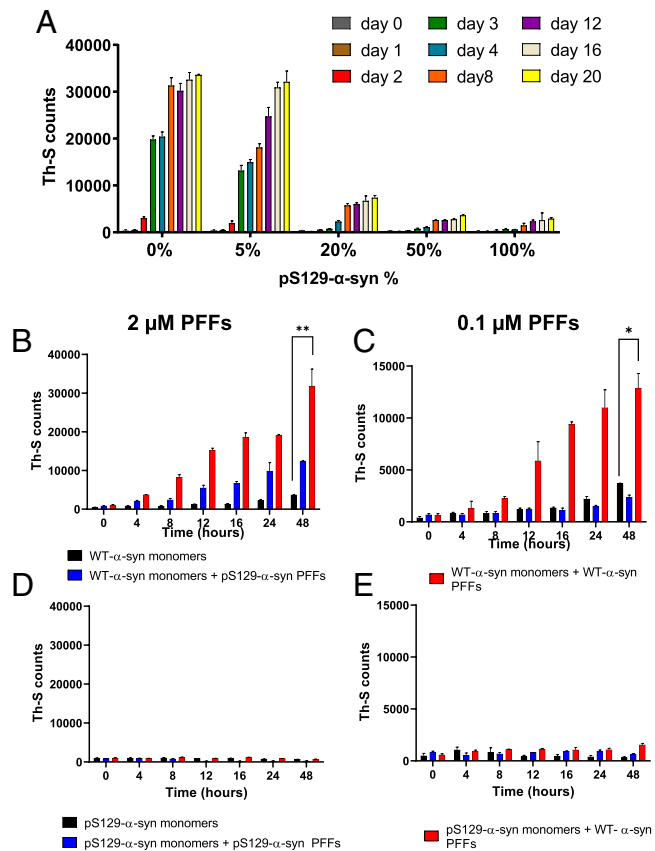


Fig. 1. Effect of pS129 on α -syn aggregation and its ability to seed the polymerization/aggregate of α -syn. (A) Monomeric α -syn was incubated in the presence of various percentages (0%, 5%, 20%, 50%, and 100%) of monomeric pS129- α -syn (final concentration 100 μ M) for 20 d at 37 $^{\circ}$ C with continuous shaking. Fibril formation was evaluated by Th-S fluorescence (RFU). The assay was performed in triplicates, and the means \pm SDs are shown. (B and C) Monomeric WT- α -syn (100 μ M) was incubated alone, with (B) 2 μ M or (C) 0.1 μ M (final concentration) of pS129 PFFs or WT PFFs for 48 h. (D and E) Samples of monomeric pS129- α -syn (100 μ M) were incubated alone or with (D) 2 μ M or (E) 0.1 μ M (final concentration) of pS129 PFFs or WT PFFs for 48 h. Fibril formation was evaluated by Th-S fluorescence (RFU). The assay was performed in triplicates, and the means \pm SDs are shown. (* P < 0.05, ** P < 0.01).

striatal brain sections from adult male α -syn knockout (KO) mice and Western blot analysis on brain tissues from human *SNCA* transgenic and *SNCA*-null mice showed no 4B1 reactivity in the KO tissues (Fig. 5 C and D).

WT- α -syn Is Predominant at Early Stages in a Seeding-Dependent Aggregation In Vitro Model of HEK Cells. To further examine when pS129 modification occurs during α -syn aggregation, whether at early or late stages, in ex vivo and in vitro models, we used the 4B1 antibody specific for WT- α -syn.

Given the central role of seeding in inducing α -syn fibril formation (30–32), seeding-dependent aggregation by mutant S129A- α -syn PFFs, and the formation of insoluble pS129- α -syn was studied in an in vitro HEK cell model expressing α -syn. Consecutive transfection with WT- α -syn and mutant S129A- α -syn PFFs led to the accumulation of insoluble pS129- α -syn, indicating that pS129- α -syn is generated at later stages following PFFs treatment, particularly after 24 to 48 h (SI Appendix, Fig. 7). In contrast, insoluble WT- α -syn detected by 4B1 showed a gradual decrease in expression, with the greatest effect at 48 h posttransfection (SI Appendix, Fig. 7). Taken together, these findings suggest

that the levels of the two forms of α -syn protein are inversely related, with insoluble WT- α -syn most abundant at early stages and gradually decreasing, with pS129- α -syn being of initial low abundance and gradually increasing commensurate with the decrease in WT- α -syn.

Slice Culture Model Displays a Maturation of Aggregates with Increasing Phosphorylation at S129 over Time. In order to investigate the temporal development in expression of pS129- α -syn in the α -syn aggregates, we employed a recently described organotypic slice culture model where α -syn aggregation is induced by injection of S129A- α -syn PFF (33). Slices were evaluated at time points ranging from 3 to 14 d following induction of aggregation in order to compare the distribution of WT- α -syn and pS129- α -syn over time (Fig. 6 A and B). While the organization of WT- α -syn and pS129- α -syn was rather homogeneous at early time points (Fig. 6A), epitopes appeared to somewhat dissociate at late time points with evident cores of WT- α -syn surrounded by pS129- α -syn in predominantly cell body aggregates (Fig. 6B). Overall analysis of the aggregates revealed a timewise decrease in both the mean fluorescence intensity (MFI) of 4B1-staining and in the area proportion of WT- α -syn in the aggregates compared to pS129- α -syn staining (Fig. 6 C and D). Consistent with previous observations, these findings suggest that α -syn becomes increasingly phosphorylated after initial protein deposition.

To further investigate how phosphorylation of α -syn corresponds with aggregate maturation, aggregates were divided into four groups based on morphology (SI Appendix, Fig. 8 A and B). For the three types of LN-like aggregates (small, intermediate, and large LNs), increasing sizes corresponded well with a concomitant increase in aggregate length, as measured by the geodesic diameter (SI Appendix, Fig. 8 B and C). For cell body aggregates, though, the geodesic diameter was smaller, as could be expected from their less elongated structure. Regarding the composition of the aggregates, small LNs constituted the vast (count-wise) majority, regardless of the time point analyzed, while the numbers of intermediate-sized LNs, large LNs, and cell body aggregates increased with time (SI Appendix, Fig. 8 D and E). Stratification of our earlier analysis of WT- α -syn MFI and area proportion by aggregate morphology revealed significant changes closely linked to aggregate type (Fig. 6 E and F). Thus, changes in the proportion of WT- α -syn relative to pS129- α -syn appear to occur alongside changes in aggregate morphology putatively linked to maturation (Fig. 6G).

pS129- α -syn Occurs at a Late Stage in Mice Injected with PFFs. To investigate the association between α -syn aggregate maturation and pS129- α -syn, mice were injected with α -syn PFFs and subjected to immunohistochemical evaluation of 4B1 compared to pS129. Early stages following PFF injection were characterized by aggregated WT- α -syn with relatively little pS129- α -syn (Fig. 7A). However, at later time points, pS129- α -syn became more evident since most of the inclusions appeared phosphorylated at week 4 postinjection (Fig. 7A). Despite the abundant pS129- α -syn positive inclusions, there were some 4B1⁺ aggregates, although to a lesser extent. Additionally, we also suggest that small undetectable non-phosphorylated aggregates may exist and maintain the pathological seeding process. These small aggregates are obvious in our ex vivo experiment as indicated in Fig. 6. Moreover, these results in a rodent propagation model further suggest that pS129- α -syn occurs secondarily to initial aggregation of WT- α -syn. In addition, negative control staining experiments including the application of only the secondary antibody have been performed, as shown in SI

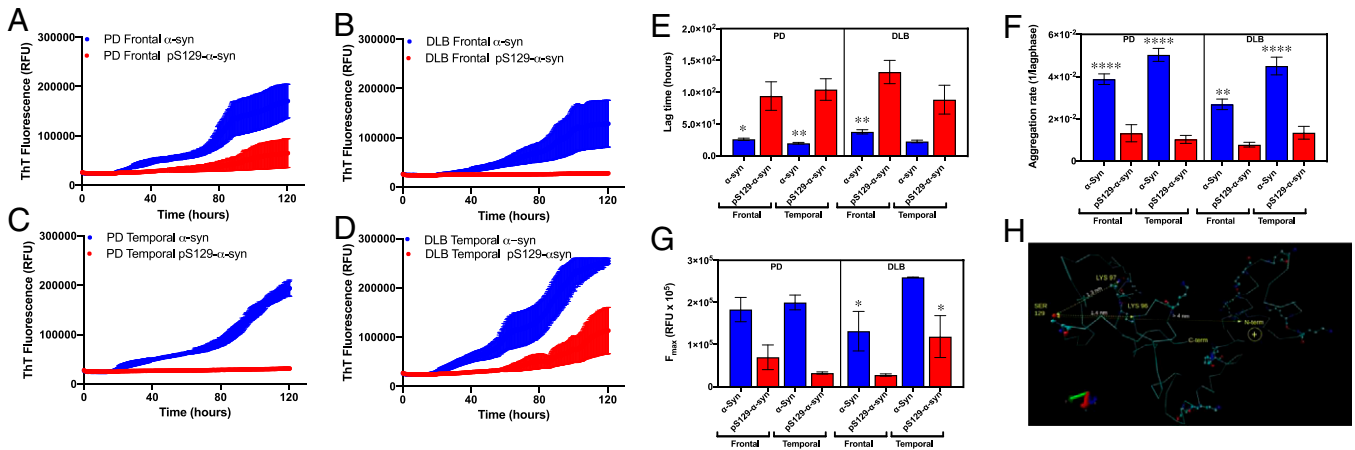


Fig. 2. Effect of pS129 on nucleation-dependent RT-QuIC assay and aggregation kinetics. The assay was performed using recombinant monomeric WT- α -syn or pS129- α -syn used as substrates in A–D. PD and DLB frontal and temporal regions. When used as a substrate, monomeric WT- α -syn showed higher seeding propensity compared to pS129- α -syn as shown by (E) shortest lag-phase, (F) highest aggregation rate, and (G) highest F_{MAX} value reached at end of the reaction. The amplification curves show the mean fluorescence in each time point with SE as shaded area. One-way ANOVA with Tukey's multiple comparison testing was used for statistical comparisons (**** $P < 0.001$; *** $P < 0.001$; ** $P < 0.01$; * $P < 0.05$). (H) Putative interactions between phosphorylated Ser-129 and Lys-96, Lys-97 (dashed lines), in addition to the N-terminal (dotted line), leading to an increase in the frequency of contacts between the C terminal and the N terminal, already observed in the unmodified protein.

Appendix, Fig. 10. Upon proteinase K (PK) treatment, the majority of the 4B1 immunopositive accumulations in the ipsilateral dorsal striatum at 2 wk post-PFF inoculation were PK resistant, as illustrated in Fig. 7B.

WT- α -syn Load Correlates Inversely with Disease Duration.

Immunohistochemical staining of PD dementia (PDD) and DLB postmortem human brain tissue demonstrated that WT- α -syn as labeled by 4B1 is found in LNs and Lewy bodies, though its load is approximately fourfold lower than total α -syn labeled by a pan- α -syn antibody (Fig. 8A). When normalized to total α -syn levels, there was no significant difference in load of 4B1 between PDD and DLB cases ($P = 0.650$); however, pS129- α -syn when normalized to total α -syn was proportionally higher in PDD cases ($U = 53$, $P = 0.025$). Furthermore, 4B1 expression in the amygdala was inversely correlated with disease duration across all cases ($r_s = -0.440$, $n = 30$, $P = 0.015$), but no relationship was observed between pS129- α -syn and disease duration ($P = 0.601$) (Fig. 8B). It is difficult to draw conclusions from the significance of these data given relationships were only identified between 4B1 and disease duration, and no relationships were observed between pS129- α -syn and disease duration. We also explored whether 4B1 was predominantly present within the core of protein aggregates and pS129- α -syn in the corona using immunofluorescence. Confocal microscopy of immunofluorescent sections demonstrated some accumulations that were positive for 4B1 but not pS129- α -syn or vice versa, but no evidence of selective labeling of the core of aggregates with 4B1 (Fig. 8C).

To determine whether the relationship between WT- α -syn and disease duration was mediated by other variables, we also evaluated whether it was associated with age at onset or concomitant Alzheimer-type pathology. We identified that 4B1 normalized to total α -syn was not correlated with Braak Tau pathology stage ($P = 0.210$) or Thal phase ($P = 0.104$); however, there was a significant positive correlation between WT- α -syn and age at onset ($r_s = 0.478$, $n = 30$, $P = 0.008$). As age at onset was strongly correlated with disease duration ($r_s = 0.783$, $n = 30$, $P < 0.001$), one could speculate that the association between WT- α -syn and age at onset is related to disease duration.

Discussion

Phosphorylation at serine 129 is one of the major PTMs of α -syn (34), and is known to increase to 90% in Lewy bodies and LNs. Based on the elevated expression of pS129- α -syn in Lewy body disease pathology, this PTM has been assumed to play a central role in the pathogenesis of Lewy body disease (35). However, there are only a few studies evaluating its disease relevance, in part due to a lack of robust tools for studying WT- α -syn. To better understand the pathogenic relevance of pS129- α -syn to Lewy body disease, we comprehensively evaluated the seeding propensity and cytotoxicity of pS129- α -syn in a range of novel model systems, in addition to human postmortem brain tissue.

Contrary to the putative pathogenic role ascribed to pS129- α -syn (12), but consistent with previous findings in a yeast model (15), the present study demonstrated that pS129 modification reduced the aggregation propensity and resultant cytotoxicity of α -syn in vitro, and occurred secondarily to WT- α -syn aggregation in in vitro, ex vivo, and in vivo models. It may be that this cellular event of pS129 modification following WT- α -syn aggregation indicates an inhibitory mechanism for α -syn aggregation or an approach for degradation of the aggregates (14, 35). Furthermore, the abundance of WT- α -syn inversely correlated with disease duration in postmortem samples, consistent with WT- α -syn being elevated early in the disease process. Taken together, our findings challenge the central pathogenic role ascribed to pS129- α -syn in Lewy body disease, instead suggesting this disease-associated modification may occur secondarily to initial protein aggregation and may even attenuate the cytotoxicity of α -syn (36).

In the present study, we report that the pS129 modification inhibits α -syn aggregation into amyloid structures and has a reduced ability to seed aggregation of α -syn as shown by Th-S binding assay. Similarly, a previous study also demonstrated that phosphorylation at serine 129 inhibits rather than promotes α -syn fibril formation in vitro (24). Using the RT-QuIC assay to evaluate aggregation propensity of α -syn, monomeric WT- α -syn demonstrated higher seeding propensity than pS129- α -syn monomers, which showed virtually no seeded aggregation when seeded with frontal or temporal cortex brain lysates from PD or DLB cases. Additionally, molecular simulations suggested that pS129 may stabilize α -syn monomers, and

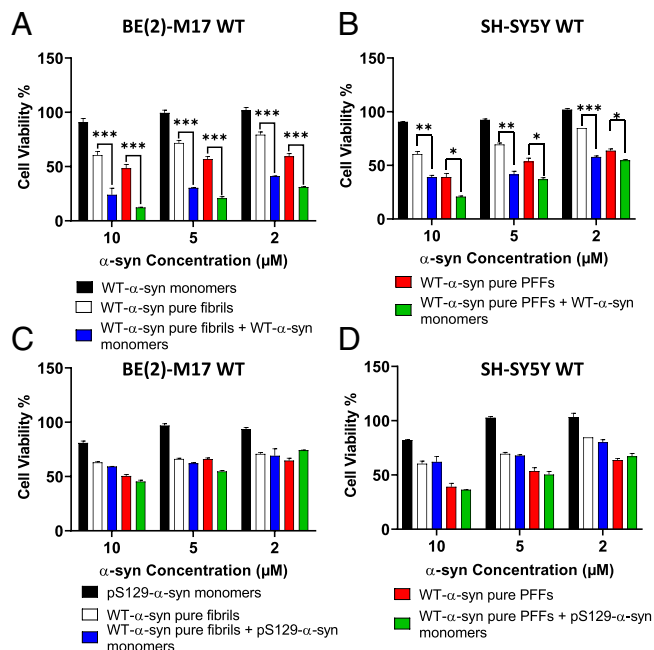


Fig. 3. Effect of WT- and pS129- α -syn seeding on the viability of neuroblastoma cells. The effect of WT- and pS129- α -syn-seeding on the viability of (A and C) BE (2)-M17-WT and (B and D) SH-SY5Y human neuroblastoma WT cells was estimated by the MTT assay. (A and C) BE (2)-M17 and (B and D) SH-SY5Y cells were treated with different concentrations of α -syn pure fibrils or pure PFFs and 1 h after treatment, monomeric WT or pS129- α -syn was added to a final concentration of 10 μ M for 48 h (average of three wells \pm SD). The results are expressed as the percentage of the control average (i.e., untreated cells) (** $P < 0.001$; ** $P < 0.01$; * $P < 0.05$).

thus resist further aggregation. When cytotoxicity was evaluated, we noted that pS129- α -syn seeding had no effect on the viability of neuroblastoma cells. Consistent with previous results that pS129 attenuates the pathogenicity of α -syn by inhibiting aggregation, *in vitro* cell models demonstrated consistent results where, in contrast to WT-, pS129- α -syn reduced α -syn seeded aggregation. Although there are conflicting results in the literature regarding the aggregation propensity and cytotoxicity of pS129- α -syn compared to WT- α -syn, our findings are in accord with some previous observations (15, 24, 37–39). Contrary to our observations, another study reported α -syn phosphorylation at serine 129 induces higher cytotoxicity in neuroblastoma cell lines (40). Furthermore, another study reported that rotenone treatment of SH-SY5Y cells caused cell death and increased expression of pS129- α -syn that was ameliorated by blocking phosphorylation by substituting serine for alanine (S129A) (11). However, it must be noted that rotenone exposure alters the structure of α -syn, thus promoting aggregation but it is unclear the extent to which these aggregates recapitulate what is observed in the human brain in Lewy body disease (41).

As part of this study, we developed and thoroughly characterized an antibody specific for the aggregated form of WT- α -syn. Our antibody was employed to study the impact of phosphorylation on α -syn seeding aggregation in established HEK cell model, organotypic slice culture model, and in mice brain sections that were injected with PFFs. In addition, this antibody was studied in human postmortem brain tissue. In an *in vitro* HEK cell α -syn-seeding model, insoluble WT- α -syn was abundant mostly at early stages following PFF treatment and gradually decreasing with time; on the other hand, pS129- α -syn was gradually increasing. Data from the organotypic slice culture model showed a time-dependent decrease in

MFI of 4B1-staining and in the area proportion of WT- α -syn in the aggregates compared to pS129- α -syn staining, proposing that α -syn becomes increasingly phosphorylated after initial protein deposition. Additionally, in mice injected with PFFs, early stages following PFF injection were characterized by aggregated WT- α -syn with pS129- α -syn more evident at later time points. Moreover, in postmortem samples, 4B1 expression in the amygdala was inversely correlated with disease duration among all cases. Taken together, these findings suggest that phosphorylation occurs subsequent to initial protein aggregation in several model systems. Although we demonstrated that 4B1 recognizes conformation-specific non-pS129- α -syn (WT- α -syn) aggregates in a number of systems, it is impossible to be sure that the same conformation is being labeled in human postmortem brain tissue due to the potential impact of epitope unmasking steps on protein structure or indeed due to partial denaturation of conformations as part of the paraffin wax-embedding process and heating sections prior to dewaxing. Nevertheless, this does not change the fact that the antibody is labeling WT- α -syn aggregates, it may suggest that the conformation in Lewy body disease brains differs from that in model systems. Future studies are warranted to precisely determine the structural properties of WT- α -syn aggregates recognized by 4B1 in Lewy body disease brain samples.

The findings from all the α -syn-seeding model systems and, to some extent, those from human brain tissue are consistent with the proposition that initial α -syn aggregation is associated with relatively low levels of pS129 but that this modification increases with time and aggregate maturity. These observations are consistent with a previous study of Lewy body structure using advanced imaging that reported pS129- α -syn on the outside of lesions (42). As increasing aggregation of α -syn is thought to be a characteristic of Lewy body disease pathology, including Lewy bodies and neurites, it is tempting to speculate that the inhibitory effect of pS129 on α -syn aggregation is likely to attenuate its pathological effects. However, as high levels of pS129- α -syn are observed in end-stage cases of Lewy body disease, it would seem that this potential protective effect of pS129 is not sufficient to fully protect the brain from neurodegeneration. Nevertheless, it is plausible to suggest that pS129 may mediate important individual factors, such as latency to symptom onset and trajectory of motor or cognitive decline, and future studies may wish to evaluate the potential role of pS129 in arresting clinical decline.

Our present findings have major implications for understanding the pathobiology of Lewy body disease and the therapeutic targeting of α -syn. It is reasonable to suggest that therapeutic targeting of α -syn aggregates should be focused on those that form early and are most associated with pathological propagation and cytotoxicity. While there is no doubt that pS129- α -syn is a useful and relatively specific marker of Lewy body disease pathology, particularly when normalized to total α -syn levels (43), WT- α -syn may be a better prognostic biomarker given that it appears to precede pS129 modification and contributes to propagation of pathology. Thus, in future studies, it will be of interest to examine the extent of nonphosphorylated α -syn aggregates and subsequent correlation with disease in transgenic models of synucleinopathy. The present data also highlight the importance of understanding the development and progression of Lewy pathology over time, and may assist in the design of future research studies to differentiate distinct α -syn species with different pathogenic roles. There is a pressing need to better understand the

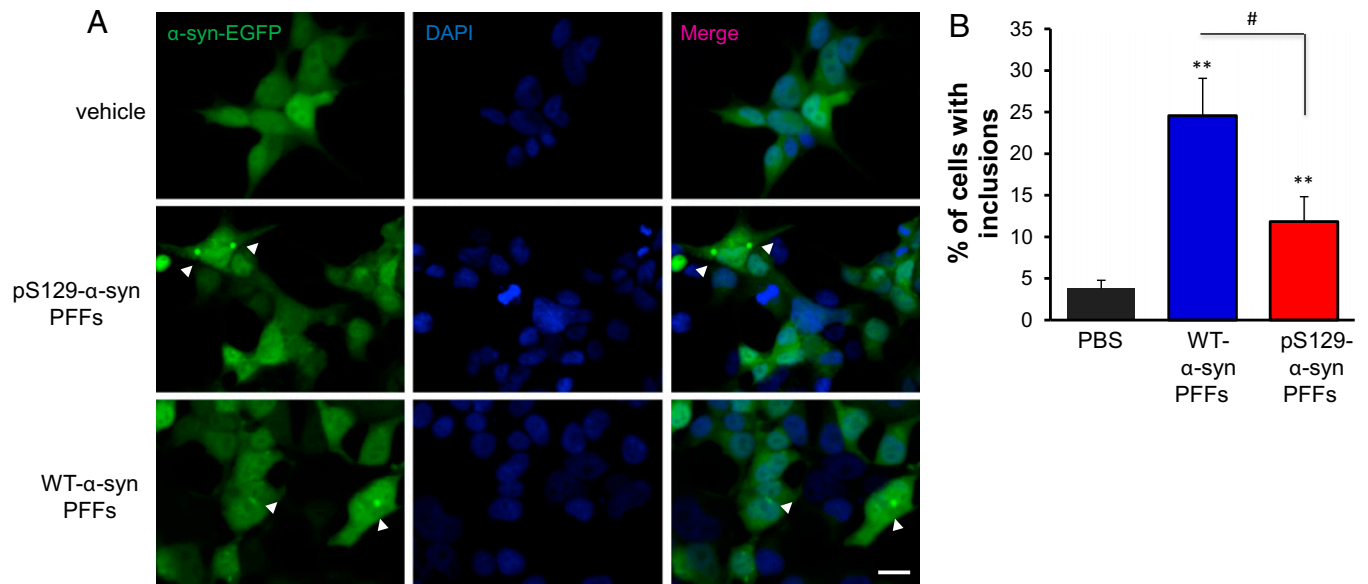


Fig. 4. Effect of pS129- α -syn PFFs in seeding the aggregation of endogenously expressed α -syn-EGFP. (A) Treatment with α -syn PFFs in a concentration of 100 nM for 4 d. Representative images of cells under the different treatments. DAPI was used for nuclear staining. (Scale bar, 10 μ m.) (B) Quantification of the percentage of cells with inclusions (>200 cells counted per condition, four independent experiments; mean \pm SD) revealed that pS129- α -syn is less potent than WT- α -syn in seeding aggregation. Arrowheads refer to α -syn-EGFP inclusions, #: comparison WT PFFs to pS129- α -syn PFFs (** P < 0.01).

temporal sequence of Lewy body formation, both for developing novel biomarkers and for understanding the cell biology of α -synucleinopathies, and thus our observations may stimulate further study into the pathogenic relevance of pS129 and other PTMs of α -syn in Lewy body disease. This is particularly important given the use of reduced levels of pS129 as an endpoint in clinical trials of potential disease-modifying drugs for Lewy body disease.

In conclusion, our findings from several approaches including α -syn-seeding model systems suggest that pS129 modification occurs secondarily to α -syn accumulation and appears to reduce the cytotoxicity and aggregation propensity of α -syn accumulations. These data have important implications for understanding disease mechanisms, prognostic biomarker discovery, drug development, and design of future neuropathological studies.

Methods

In Vitro Phosphorylation of α -syn. As previously reported, full-length recombinant human α -syn was expressed and purified (44). Purified α -syn was phosphorylated at S129, as described previously (43). Briefly, 1 μ g of Polo-like kinase 2 (PLK2) protein was added to 1.44 mg/mL (100 μ M) α -syn in kinase reaction buffer (20 mM HEPES, 1.09 mM ATP, 2 mM DTT, 10 mM MgCl₂, pH 7.4). Reaction mixture was incubated at 30 °C for 24 h.

Seeded Polymerization Assay. The aggregation of monomeric WT- or pS129- α -syn with or without addition of PFFs was conducted as previously described (45). As described above, the PFFs (WT or pS129) were prepared by fragmenting mature α -syn fibrils via sonication. Monomeric α -syn (100 μ M) was seeded with different PFF concentrations under incubation at 37 °C with continuous shaking. The fibril formation was assessed by the Th-S binding assay.

RT-QuIC Assay. The RT-QuIC reaction buffer was composed of 0.1 M piperazine-N,N'-bis (ethanesulfonic acid) (Pipes; pH 6.9), 0.1 mg/mL recombinant α -syn and 10 μ M thioflavin-T (Th-T). Reactions were performed in triplicates in a black 96-well microplate with a clear bottom (Nunc) with 85 μ L of the reaction mix loaded into each well together with 15 μ L of 0.1 mg/mL TBS-soluble fractions. The plate was then sealed with a sealing tape (ThermoFisher) and incubated at 37 °C for 120 h in a BMG FLUOstar OMEGA plate reader with intermittent cycles of 1-min shaking (500 rpm, double orbital) and 15-min rest

throughout the indicated incubation time. Th-T fluorescence measurement, expressed as arbitrary relative fluorescence units (RFU), was taken with a bottom read every 15 min using 450 \pm 10-nm (excitation) and 480 \pm 10-nm (emission) wavelengths. A positive RT-QuIC signal is defined as RFU more than 5 SD units (RFU > 5 SD) above the mean of initial fluorescence at 120 h. The sample was considered positive if two or more of the replicates were positive, otherwise the sample was classified as negative. The relative seeding activities of the assayed samples were presented by graphing fluorescence readouts against assay time. For each sample, we calculated three quantitative measures that can be used to analyze the RT-QuIC data: 1) the lag-phase (RFU > 5 SD); 2) the amyloid formation rate, expressed as the inverse (1/time to threshold) of the lag-phase (46); 3) and the maximum fluorescence value (F_{MAX}) measured at the end of the RT-QuIC reaction. For RT-QuIC-negative samples, the lag-phase was assigned as 150 h.

Molecular Dynamics Modeling. For molecular dynamics (MD) modeling, 4,000 no-AcAS NMR structures (47) were clustered in six representatives, covering almost three-quarters of the protein's conformations (48). One acetyl group was manually added to the N terminus of each representative. Each representative was inserted in a water box using a 10 Å buffer zone of solvent around any atom of the protein. The Amber ff99SB force fields (49) with ILDN modification (50) and the TIP3P water model were used for the protein and for the solvent, respectively. The systems were neutralized by adding 10 Na⁺ ions. Periodic boundary conditions were applied. Electrostatic interactions were calculated using the Particle Mesh-Ewald (PME) method. All bond lengths were constrained by the LINCS algorithm and an integration step of 2 fs was set for all of the MD calculations. Constant temperature and pressure conditions were achieved by coupling the system with a Nosé-Hoover thermostat (51) and an Andersen-Parrinello-Rahman barostat. The systems were geometry-optimized and then equilibrated at 300 K and 1 atm by performing 1 ns of MD-based annealing and 1 ns of constant temperature MD. Next, each representative underwent the replica exchange with a solute tempering (REST2) (52, 53) -enhanced sampling method at room conditions. For each REST2 simulation, 32 replicas were generated in the temperature range from 300 to 500 K. Therefore, a total of six 15-ns-long independent REST2 simulations were generated. We calculated several properties from the protein's conformational ensemble, obtained by cumulating the six lowest temperature replica trajectories: 1) CSs and CD spectra, using the SHIFTX (54) and the DichroCalc codes (55), respectively; 2) RH, gyration radii (R_g), and compaction factors (C_F) (56, 57). The structure selected is the ones featuring the best agreement with the CSs, also showing good agreement with CD and RH.

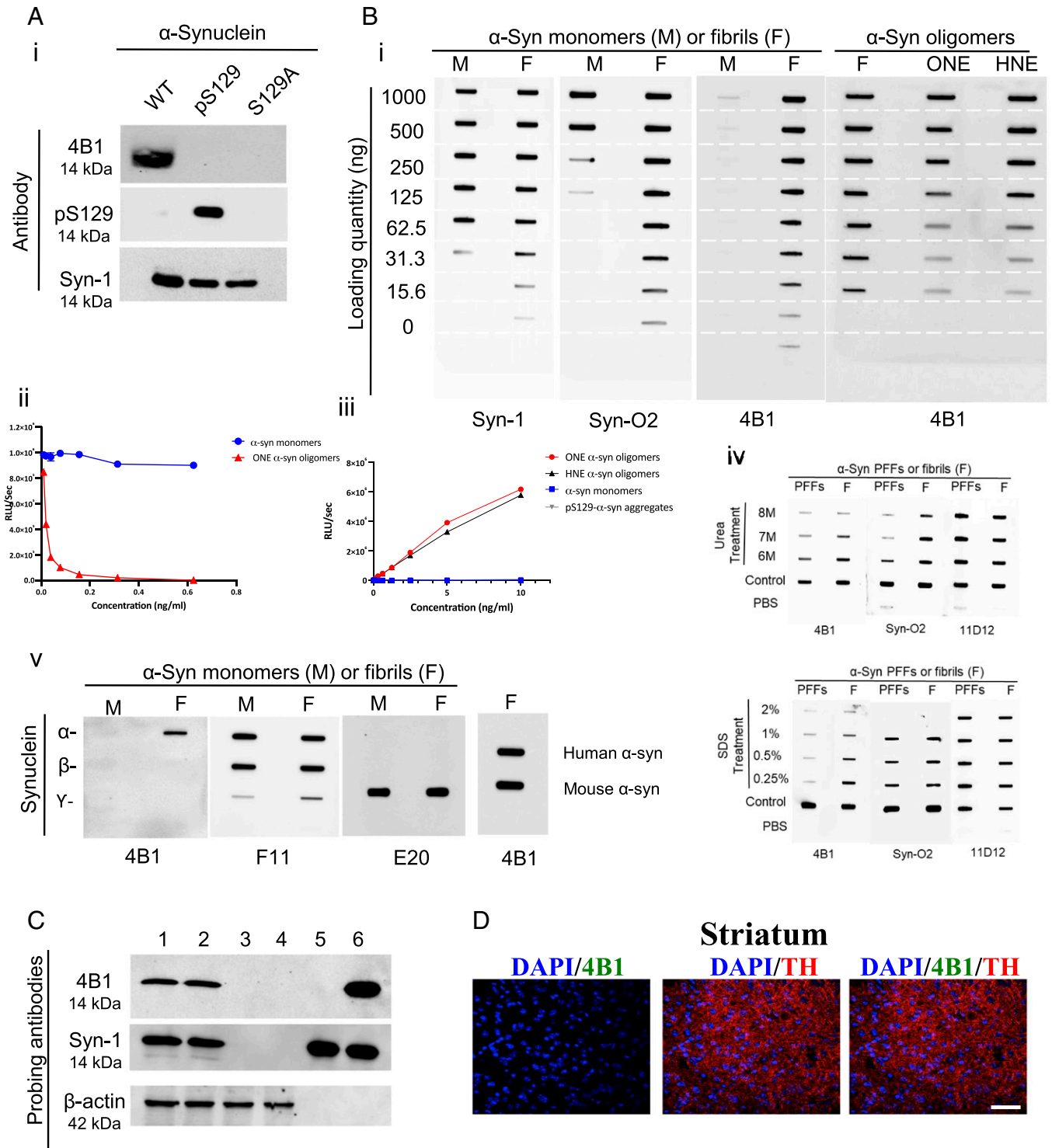


Fig. 5. Purity and specificity of 4B1 toward WT- α -syn aggregates. (A) Fifty nanograms of recombinant WT-, pS129-, or S129A- α -syn was loaded on 15% SDS gels and transferred to nitrocellulose membranes for Western blotting for 4B1, in-house pS129, and Syn-1. (B, i) Analysis of filter retardation using monomeric- (M) or fibrillar- (F) α -syn coated on nitrocellulose membranes and detected with 4B1, Syn-1, and Syn-O2. Reactivity of 4B1 toward different α -syn aggregates including fibrils, ONE, or HNE (ii) 4B1 preincubated with monomers or ONE-oligomers and tested against precoated monomeric- α -syn in inhibition ELISA. (iii) Sandwich-ELISA showing the reactivity of 4B1 toward monomers or different α -syn aggregates. (iv) Specificity of 4B1 toward WT- α -syn aggregates. PFFs and fibrils were treated for 6 h with increasing concentrations of denaturing urea and SDS, with 4B1 detecting the aggregated forms of α -syn. (v) Filter retardation assessment for 4B1 reactivity toward α -syn fibrils. F11 detects α - or β -syn, whereas the antibody E20 detects γ -syn. Filter retardation analysis of 4B1 reactivity toward human (H- α -syn) or mouse (M- α -syn) fibrils. (C) Ten micrograms of brain lysates from human SNCA transgenic (lanes 1 and 2) and SNCA-null mice (lanes 3 and 4) were immunoblotted using antibodies specific to WT- α -syn (4B1) and total α -syn (Syn-1). Recombinant pS129- α -syn (rpS129- α -syn, lane 5) and recombinant α -syn (α -syn, lane 6) proteins were loaded (50 ng) as positive controls. Reimmunoblotting with β -actin antibody was performed to normalize the amount of loaded proteins. (D) Immunofluorescence images of striatal brain sections from adult male α -syn KO mice, showing no 4B1 or pS129 immunoreactivity in the tyrosine hydroxylase (TH, red) -positive dopaminergic fibers (63 \times magnification). (Scale bar, 50 μ m).

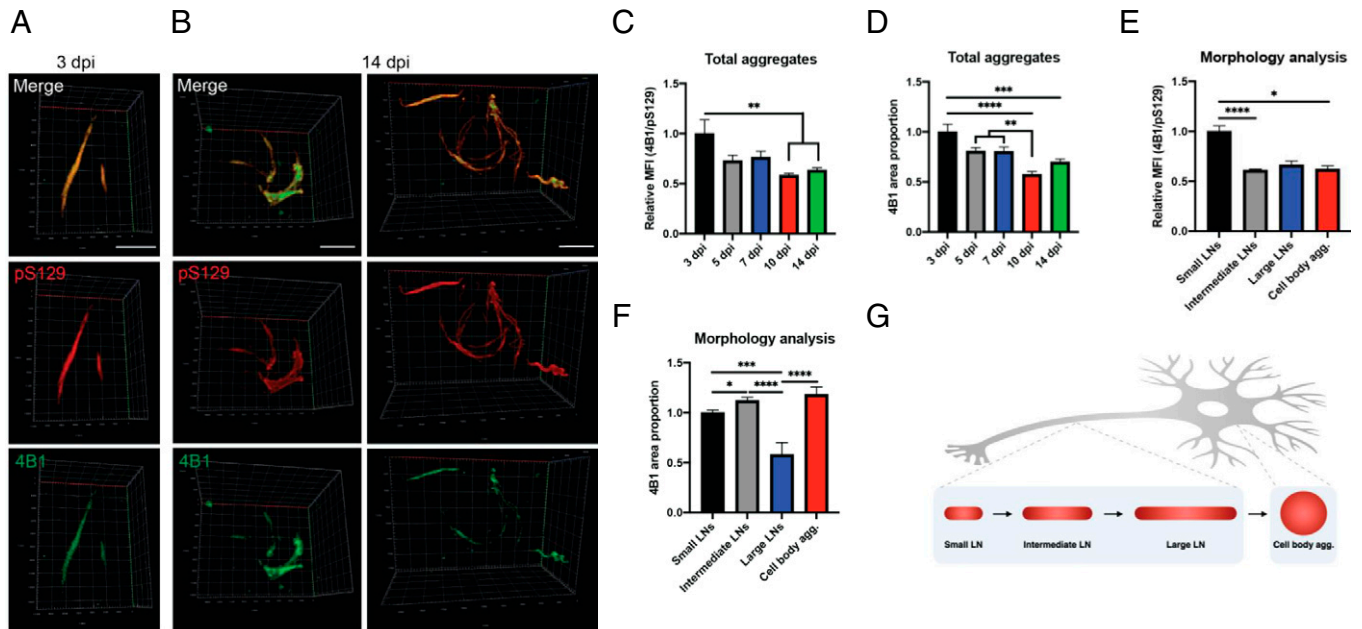


Fig. 6. Analysis of α -syn aggregates in organotypic slice culture model after injection of S129A- α -syn PFF. (A and B) Representative 3D renderings from z-stack acquisitions of aggregates in the organotypic hippocampal slice cultures at 3 d postinjection (dpi) of PFF (A) and 14 dpi (B), stained for WT- α -syn with 4B1 (green) and pS129- α -syn with D1R1R Cell Signaling pS129 (red). (Scale bars, 5 μ m.) Channel curves were adjusted to approximately equal maximum intensity of the two stainings. (C) Relative MFI of WT- vs. pS129- α -syn staining in the total population of aggregates. (D) Area proportion of WT- α -syn in the total population of aggregates. (E) Relative MFI of WT- vs. pS129- α -syn staining in each type of aggregate (small LNs, intermediate LNs, large LNs, and cell body inclusions), all time points collapsed. (F) Area proportion of WT- α -syn in each type of aggregate, all time points collapsed. (G) Schematic illustration of the putative maturation of aggregates with changing morphology. All graphs are displayed as mean \pm SEM, normalized to the first bar (* P < 0.05, ** P < 0.01, *** P < 0.001, **** P < 0.0001).

HEK293- α -syn-EGFP Cell Line Generation. HEK293 cells were transfected with a plasmid encoding human WT- α -syn fused to EGFP, at the C terminus, driven by the cytomegalovirus promoter. The plasmid contained a selection marker for the antibiotic geneticin (G418), which was used for the selection of the stable transformants. Protein expression was confirmed by Western blot analysis and fluorescence microscopy. A clonal HEK293- α -syn-EGFP cell line was selected and used for subsequent experiments. Cells were maintained in DMEM media supplemented with 10% Fetal Bovine Serum Gold (FBS) (PAA) and 1% penicillin-streptomycin (PAN). The cells were grown at 37 $^{\circ}$ C in an atmosphere of 5% CO₂. For the seeding experiments, cells were plated on 13-mm glass coverslips in 24-well plates and incubated in 5% FBS-media. The following day, α -syn PFFs were prepared in reactions of 150 μ L per tube diluted in PBS, fragmented by sonication (53), and then added to cells at final concentration of 100 nM. Control cells were exposed to vehicle only (PBS). Cells were further incubated for 4 d, washed with PBS, and fixed with 4% PFA for 20 min at room temperature, followed by nuclei staining with DAPI (Sigma-Aldrich, D8417) (1:5,000 in DPBS) for 10 min. After a final wash, coverslips were mounted using Mowiol (Sigma Aldrich) and subjected to fluorescence microscopy. The proportion of cells with α -syn inclusions within the population was then determined by counting. For quantification of aggregation, at least 200 cells were counted per variant and per experiment. Images were acquired using a 63 \times objective, and analyzed using LAS AF v.2.2.1 (Leica Microsystems) software.

Tissue Culture of HEK293 Human Embryonic Kidney Cells. WT HEK293 cells were grown in Dulbecco's MEM-high glucose (Gibco) supplemented by 15% FBS (Gibco) and 1% penicillin-streptomycin (Gibco) and incubated at 37 $^{\circ}$ C in a 5% CO₂/95% air humidified incubator. After plating HEK cells overnight in six-well plates, cells were transfected with 2 μ g of WT- α -syn plasmid DNA by lipofectamine 3,000 reagent (Invitrogen) (58). One group of α -syn expressing HEK cells was similarly transfected again with 4 μ g of mutant serine 129 to alanine (S129A) PFFs the following day.

HEK cells were lysed, at 6, 12, 24, and 48 h post-PFFs transfection, initially with 1% Triton X-100 in 50 mM Tris, 150 mM NaCl (pH 7.6) containing protease and phosphatase inhibitors to obtain soluble fractions. The pellet was further lysed with 1% SDS in 50 mM Tris, 150 mM NaCl (pH 7.6) with complete inhibitors to attain insoluble fractions. Protein concentration was determined by BCA protein assay (Pierce) prior to analysis on 12% SDS/PAGE and immunoprob-

ing with appropriate antibodies. These include monoclonal antibody against pS129- α -syn (ab51253, Abcam), mouse monoclonal antibody against α -syn Syn1 (BD Biosciences), and WT- α -syn (4B1) in addition to mouse monoclonal antibody C4 against β -actin (Sc-47778, Santa Cruz Biotechnology) as a protein loading control. Blots were subsequently incubated with horseradish peroxidase conjugated with anti-rabbit and anti-mouse IgG (Jackson ImmunoResearch), and proteins were detected with LiCOR system.

Organotypic Hippocampal Slice Cultures. Organotypic hippocampal slice cultures were created from P7 C57Bl6/J mouse pups and injected with S129A-mutated human α -syn PFFs, as previously described (33), and cultured according to Stoppini et al. (59). At various time points, tissue was fixed according to Gogolla et al. (60) and stored at 4 $^{\circ}$ C until all tissue had been collected. Slices were permeabilized in 0.5% Triton X-100 in PBS and blocked in 10% BSA. Primary antibodies against pS129- α -syn (rabbit mAb D1R1R, Cell Signaling, #23706; 1:1,000) and WT- α -syn (mouse 4B1, 200 ng/mL) were diluted in 5% BSA and applied overnight at 4 $^{\circ}$ C. After washing 6 \times 15 min in 1 \times TBS + 0.3% Triton X-100, secondary Alexa-Fluor antibodies (goat anti-mouse 488, #A11001, and goat anti-rabbit 568, #A11036) were diluted 1:2,000 and supplemented with DAPI (5 μ g/mL; Th. Geyer) in 5% BSA and applied for 3 h at room temperature. Washing was repeated and slices were mounted using DAKO Fluorescent Mounting Medium (Dako, S3023).

Immunofluorescence was evaluated on a Zeiss AxioObserver 7 inverted microscope fitted with an ApoTome to increase z-plane resolution. For quantification of the distribution of pS129- α -syn vs. WT- α -syn in aggregates, 63 \times images covering the aggregates were taken (5 to 20 images per slice depending on the amount of aggregation). Images were analyzed in Fiji (NIH) in order to compute total phosphorylated and nonphosphorylated aggregate area proportions and mean fluorescence intensity of pS129 aggregates and WT- α -syn aggregates, as well as analyses stratified by aggregate morphology and subregion localization. For each image, aggregates were first defined by their pS129-staining, with an initial uneven background subtraction using the rolling ball algorithm (set to 50 pixels), followed by thresholding using the AutoThreshold plugin (method = maxEntropy). Then, 4B1⁺ aggregates were defined inside the pS129-defined aggregates, using the same steps as for pS129⁺ aggregates. Aggregates were analyzed using the Extended Particle Analyzer in the BioVoxell Toolbox (46) and stratified by morphology (small, intermediate, and long LN-like plus cell body

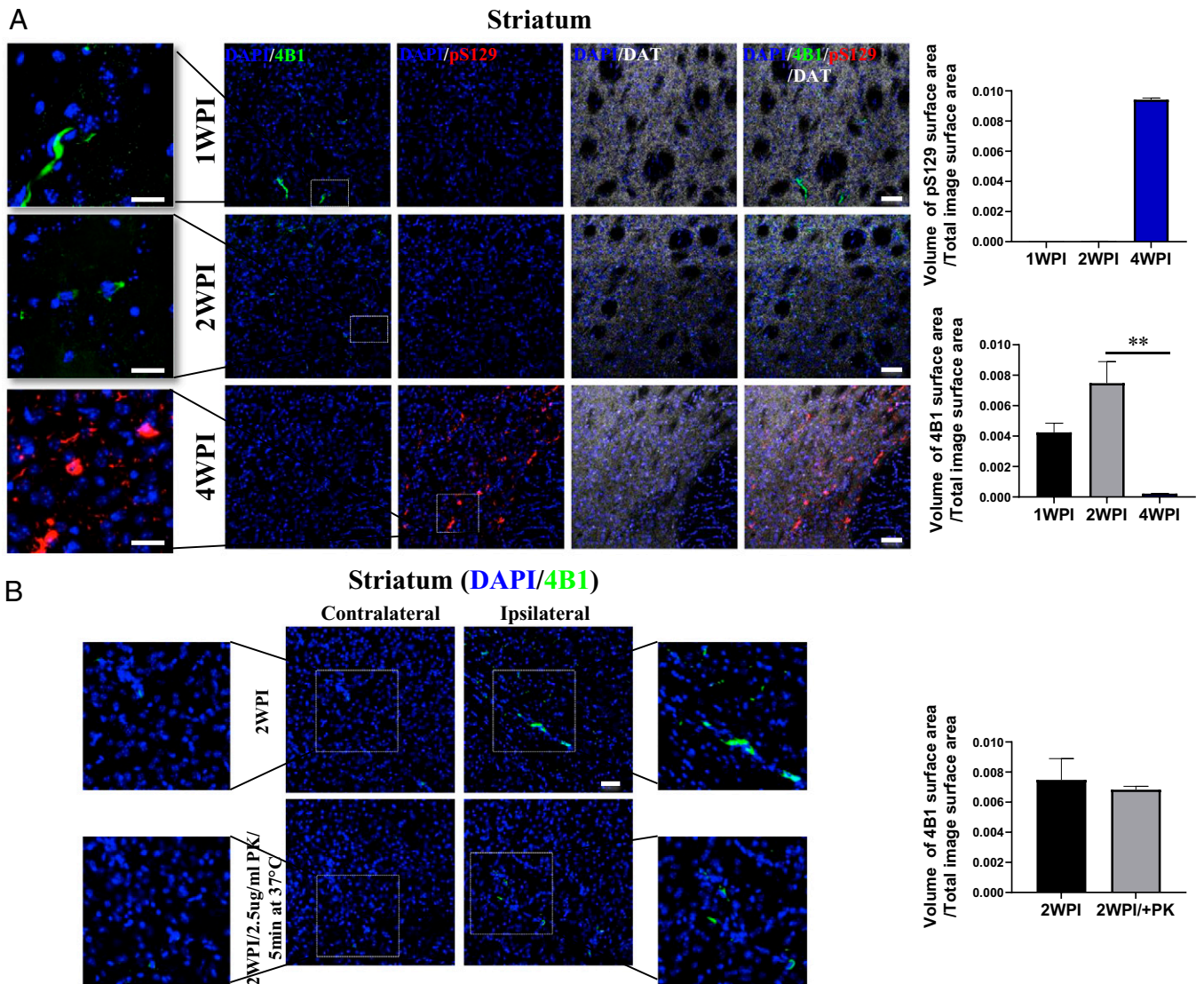


Fig. 7. Immunofluorescence analysis on brain sections from mice injected with recombinant α -syn PFFs. (A) Adult C57Bl6 male mice were inoculated with 2.6 μ g mouse PFF in the right dorsal striatum and were killed 1 (1WPI), 2 (2WPI), or 4 wk (4WPI) postinjection. Immunofluorescence images showing the 4B1 (green, aggregated WT- α -syn), Abcam ab51253 pS129 (red, phosphorylated α -syn) and DAT (white) immunoreactivity in the ipsilateral striatum at 1, 2, and 4 wk postinjection (40 \times magnification). (Scale bars, 50 μ m.) The zoomed captions were obtained with 63 \times lens zoom 2.3. (Scale bars, 25 μ m.) Graph showing the relative volume of the 4B1 and pS129 immunopositive accumulations in the ipsilateral dorsal striatum at 1, 2, and 4 wk post PFF inoculation. $n = 3$ mice per group, 3 serial striatal levels per mouse (** $P < 0.01$). (B) Immunofluorescence images showing the PK-resistant 4B1 (green) accumulations in the ipsilateral striatum at 2 wk post injection (40 \times magnification). (Scale bar, 50 μ m.) The zoomed captions were obtained with 63 \times lens zoom 2.3. (Scale bar, 25 μ m.) Graph showing the relative volume of the PK-resistant 4B1 immunopositive accumulations in the ipsilateral dorsal striatum at 2 wk post-PFF inoculation. $n = 3$ mice, 3 serial striatal levels per mouse (** $P < 0.01$).

aggregates). The exact parameters defining each type of aggregate can be found in *SI Appendix, Fig. 8A*. The various aggregate types were counted at each time point, and for each aggregate, its length was approximated using the geodesic diameter from the MorphoLibJ-plugin in Fiji (47). Finally, mean fluorescence intensity of pS129 and 4B1 inside the aggregates was computed. A total of 31 slices were used for analysis, and more than 5,000 aggregates were included in the analysis.

Representative images were taken as z-stacks on the 63 \times objective, and three-dimensional (3D) renderings were made in Zen 2.3 (Zeiss). For the 3D renderings, channel curves for pS129 (red) and 4B1 (green) were adjusted so that maximum intensity was approximately equal between the two channels, to avoid any variance in staining distribution due to differences in antibody dilutions, affinity, or microscope imaging settings. Thus, distinctions in pS129- and 4B1-staining should reflect actual differences in epitope distribution, although this setup slightly underestimates pS129-staining of the aggregates.

WT Mice Injected with Recombinant α -syn PFFs. WT C57Bl6 mice 2 to 4 mo old (Jackson Laboratory) were housed in the animal facility of the Biomedical Research Foundation at the Academy of Athens in a room with a controlled light/dark cycle (12-h light/12-h dark) and free access to food and water. Adult male

WT C57Bl6 mice were subjected to unilateral striatal injections under general isoflurane anesthesia by an apparatus adjusted to the stereotaxic frame (Kopf Instruments). Right dorsal striatum was targeted using the following coordinates from bregma: anteriorposterior +0.5 mm, mediolateral -1.4 mm, and dorsoventral in two depths -3.2 mm and -3.4 mm according to mouse brain atlas. A total of 2.6 μ g (2 μ L) of mouse recombinant α -syn PFFs were injected at a constant flow rate of 0.3 μ L/min. Equal volume of dPBS1X was used for control animals. An interval of 5 min was maintained between the two dorsoventral depths and the needle was slowly removed 5 min after the injection procedure was completed. For immunohistochemical analysis, mice were transcardially perfused under isoflurane anesthesia, followed by ice-cold 4% PFA, 2 wk poststereotaxic injections. Following fixation, the brains were dehydrated by sequential incubation in 15% and 30% sucrose, snap frozen in isopentane at -50 $^{\circ}$ C and stored at -80 $^{\circ}$ C. Free-floating cryostat-cut coronal sections (30 μ m) covering the whole nigrostriatal axis were stained with antibodies against rabbit pS129- α -syn (ab51253, Abcam), mouse 4B1, and rat DAT (MAB369, Millipore). The sections were treated with antigen retrieval solution (citrate buffer, pH = 6) at 80 $^{\circ}$ C for 20 min. To validate whether pS129 $^{+}$ α -syn accumulations were PK-resistant, sections were incubated with PK (Sigma-Aldrich) 2.5 μ g/mL in PBS

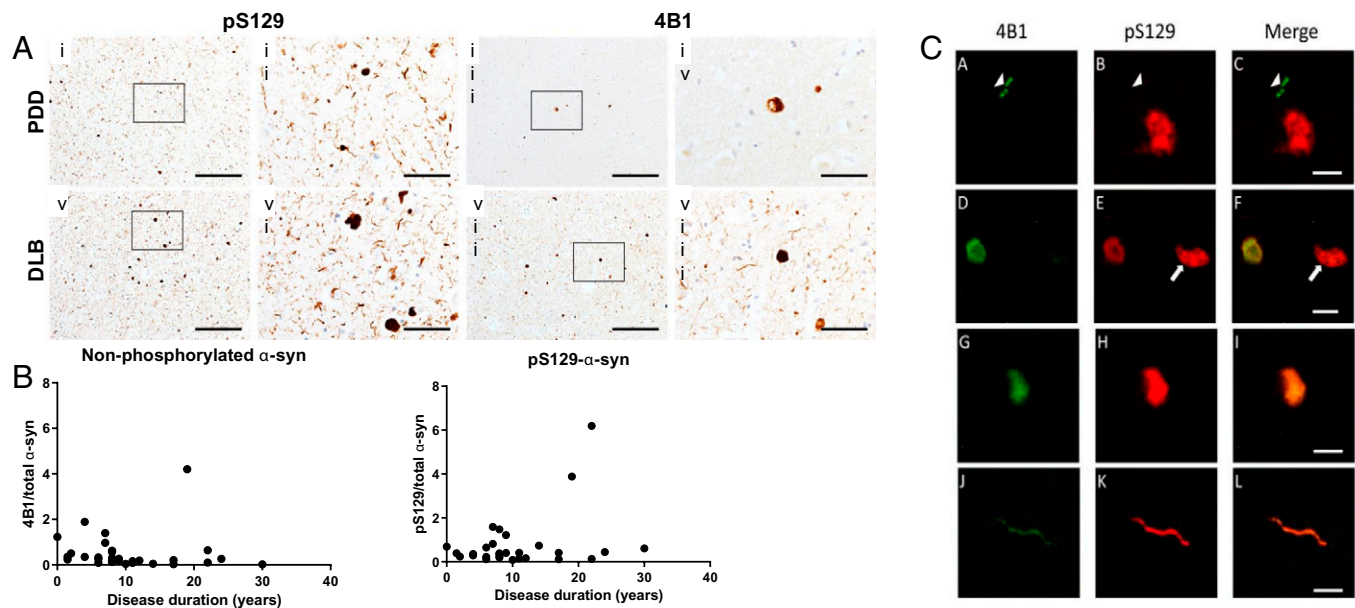


Fig. 8. Expression of WT- and pS129- α -syn in postmortem human brain tissue. (A) Representative staining of the amygdala of PDD (*i-iv*) and DLB (*v-viii*) cases stained with in-house pS129 and 4B1 on consecutive sections. Sections were imaged at precisely the same location on both slides. (Scale bars, 200 μ m [*i, ii, v, vi*] and 50 μ m [*iii, iv, vii, viii*].) (B) WT- α -syn expression in the amygdala was evaluated with disease duration across all cases, showing an inverse relationship (-0.44 , $n = 30$, $P = 0.015$). (C) Immunofluorescent staining demonstrated some fine neurites labeled with 4B1 but not pS129 (A-C), with some typically larger structures immunoreactive for pS129 but not 4B1 (D-F). However, the many aggregates were immunoreactive for both 4B1 and pS129 (G-L), with no indication of 4B1 labeling the outer precipice of aggregates preferentially. (Scale bars, 25 μ m in A-C and 10 μ m in D-L.)

for 10 min at 25 °C (Fig. 7B). Fluorescent images were obtained in a Leica SP5-II confocal microscope. A protocol with sequential image acquisition was used. For the quantification of 4B1 immuno-reactivity, raw confocal images of serial striatal sections of PFF-inoculated mice were analyzed using the surface function of the Imaris 9.1.2 software. The relative volume of the 4B1 surface area was normalized to the total surface area of the image.

Experimental procedures using mice were carried out in accordance with the institutional ethical rules and regulations of the Biomedical Research Foundation at the Academy of Athens.

Immunohistochemistry and Immunofluorescence. Formalin-fixed paraffin-embedded brain tissue from the amygdala was obtained postmortem from patients with PDD and DLB (SI Appendix, Table S1). Sections (6 μ m) were cut and stained with 4B1 (250 ng/mL), in-house pS129 (100 ng/mL), or pan- α -syn (5 μ g/mL; KM51, Leica Novocastra) antibodies and detected using conventional immunohistochemistry with Menarini MenaPath X-Cell Linked HRP detection kits (Menarini Diagnostics). Regions of interest were imaged on a Zeiss A.1 microscope (Zeiss) from five (amygdala) regions and percentage area immunoreactive was evaluated using ImagePro software. The same regions were evaluated on serial sections with different antibodies and compared between cases and across sections, and compared to clinical data obtained during life.

Sections were dewaxed and rehydrated through a series of alcohol solutions prior to epitope unmasking with PK (20 μ g/mL in Tris-EDTA pH8 buffer) for 20 min at 37 °C. Sections were blocked with 10% normal goat serum in TBS-T for 1 h before overnight incubation at 4 °C in the primary antibody solution comprised of either 4B1 (Ms IgG1, 2 μ g/mL), in-house pS129 (Ms IgG2a, 1 μ g/mL) and Abcam ab51253 pS129 (Rb IgG, 5 μ g/mL). Secondary antibodies were isotype-specific goat antibodies against mouse IgG1-546 (#A-21123), mouse IgG2a-488 (#A-21131) or rabbit IgG-647 (#A27040; Thermo Scientific), as appropriate, and all were used at a dilution of 1:100 in 10% normal goat serum in TBS-T for 1 h at room temperature. Sections were then washed and incubated in 1% Sudan Black B solution for 7 min at room temperature to eliminate auto-fluorescence, prior to mounting with ProLong Gold antifade (Thermo Scientific). Sections were imaged on a Leica SP8 confocal microscope (Leica).

Statistical Analyses. Using the GraphPad Prism software (version 8.3.0), statistical analyses were done using the Student's *t* test when comparing two groups. For comparison of three or more groups, statistical analysis was performed using

one-way ANOVA, followed by Tukey's multiple comparison test for the MTT cell viability, Th-S, and RT-QuIC assays or Holm-Sidak test for the organotypic hippocampal slice cultures. Correlational analyses for human postmortem data used Spearman's rank-order correlation coefficient, as data were unsuitable for parametric analyses. The data are presented as mean \pm SD and represents results from at least three independent experiments.

Data Availability. All study data are included in the main text and SI Appendix.

ACKNOWLEDGMENTS. We thank Prof. Michael Schlossmacher (University of Ottawa, Canada) for providing SNCA transgenic and SNCA-null mouse brain tissues, and Dr. Giulia Rossetti (Forschungszentrum Jülich, Germany) and Prof. Claudio Fernandez (Universidad Nacional de Rosario, Argentina) for their contributions to the modelling of the effect of S129 phosphorylation. The work conducted by the O.M.A.E.-A. laboratory was supported by the Qatar Biomedical Research Institute under Internal Grant VR98. D.E. is funded by an Alzheimer's Research UK Fellowship (ARUK-RF2018C-005). Human brain tissue was provided by Newcastle Brain Tissue Resource, which is funded in part by a grant from the UK Medical Research Council (G0400074), by National Institute for Health Research Newcastle Biomedical Research Centre awarded to the Newcastle upon Tyne NHS Foundation Trust and Newcastle University, and by a grant from the Alzheimer's Society and Alzheimer's Research UK as part of the Brains for Dementia Research Project. P.H.J. is funded by Lundbeck Foundation Grants R223-2015-4222 and R248-2016-2518 for the Danish Research Institute of Translational Neuroscience (DANDRITE), Nordic-European Molecular Biology Laboratory Partnership for Molecular Medicine, Aarhus University, Denmark.

Author affiliations: ^aNeurological Disorders Research Center, Qatar Biomedical Research Institute, Hamad Bin Khalifa University, Qatar Foundation, Doha 34110, Qatar; ^bDepartment of Biochemistry, College of Medicine and Health Science, United Arab Emirates University, Al Ain, United Arab Emirates; ^cTranslational and Clinical Research Institute, Newcastle University, Newcastle upon Tyne NE1 7RU, United Kingdom; ^dDanish Research Institute of Translational Neuroscience, Aarhus University, 8000 Aarhus, Denmark; ^eDepartment of Biomedicine, Aarhus University, 8000 Aarhus, Denmark; ^fDepartment of Experimental Neurodegeneration, Center for Biostructural Imaging of Neurodegeneration, University Medical Center Göttingen, 37075 Göttingen, Germany; ^gCenter of Basic Research, Biomedical Research Foundation of the Academy of Athens, 115 27 Athens, Greece; ^hDepartment of Physics, Rheinisch Westfälische Technische Aachen University, 52062 Aachen, Germany; ⁱComputational Biomedicine, Institute of Advanced Simulation IAS-5, 52425 Jülich, Germany; ^jComputational

1. K. A. Jellinger, Neuropathological spectrum of synucleinopathies. *Mov. Disord.* **18** (suppl. 6), S2–S12 (2003).
2. T. F. Outeiro *et al.*, Dementia with Lewy bodies: An update and outlook. *Mol. Neurodegener.* **14**, 5 (2019).
3. M. G. Spillantini *et al.*, Alpha-synuclein in Lewy bodies. *Nature* **388**, 839–840 (1997).
4. M. Farrer *et al.*, Comparison of kindreds with parkinsonism and alpha-synuclein genomic multiplications. *Ann. Neurol.* **55**, 174–179 (2004).
5. A. B. Singleton *et al.*, Alpha-synuclein locus triplication causes Parkinson's disease. *Science* **302**, 841 (2003).
6. P. Ibáñez *et al.*, Causal relation between alpha-synuclein gene duplication and familial Parkinson's disease. *Lancet* **364**, 1169–1171 (2004).
7. H. Fujiwara *et al.*, Alpha-synuclein is phosphorylated in synucleinopathy lesions. *Nat. Cell Biol.* **4**, 160–164 (2002).
8. J. P. Anderson *et al.*, Phosphorylation of Ser-129 is the dominant pathological modification of alpha-synuclein in familial and sporadic Lewy body disease. *J. Biol. Chem.* **281**, 29739–29752 (2006).
9. P. J. Kahle, M. Neumann, L. Ozmen, C. Haass, Physiology and pathophysiology of alpha-synuclein. Cell culture and transgenic animal models based on a Parkinson's disease-associated protein. *Ann. N. Y. Acad. Sci.* **920**, 33–41 (2000).
10. W. W. Smith *et al.*, Alpha-synuclein phosphorylation enhances eosinophilic cytoplasmic inclusion formation in SH-SY5Y cells. *J. Neurosci.* **25**, 5544–5552 (2005).
11. N. Sugeno *et al.*, Serine 129 phosphorylation of alpha-synuclein induces unfolded protein response-mediated cell death. *J. Biol. Chem.* **283**, 23179–23188 (2008).
12. M. Karampetsou *et al.*, Phosphorylated exogenous alpha-synuclein fibrils exacerbate pathology and induce neuronal dysfunction in mice. *Sci. Rep.* **7**, 16533 (2017).
13. O. S. Gorbatyuk *et al.*, The phosphorylation state of Ser-129 in human alpha-synuclein determines neurodegeneration in a rat model of Parkinson disease. *Proc. Natl. Acad. Sci. U.S.A.* **105**, 763–768 (2008).
14. A. Oueslati, K. E. Paleologou, B. L. Schneider, P. Aebischer, H. A. Lashuel, Mimicking phosphorylation at serine 87 inhibits the aggregation of human alpha-synuclein and protects against its toxicity in a rat model of Parkinson's disease. *J. Neurosci.* **32**, 1536–1544 (2012).
15. S. Tenreiro *et al.*, Phosphorylation modulates clearance of alpha-synuclein inclusions in a yeast model of Parkinson's disease. *PLoS Genet.* **10**, e1004302 (2014).
16. N. R. McFarland *et al.*, Alpha-synuclein S129 phosphorylation mutants do not alter nigrostriatal deposition in a rat model of Parkinson disease. *J. Neurochem. Exp. Neurol.* **68**, 515–524 (2009).
17. S. Azeredo da Silveira *et al.*, Phosphorylation does not prompt, nor prevent, the formation of alpha-synuclein toxic species in a rat model of Parkinson's disease. *Hum. Mol. Genet.* **18**, 872–887 (2009).
18. V. Delic *et al.*, Sensitivity and specificity of phospho-Ser129 alpha-synuclein monoclonal antibodies. *J. Comp. Neurol.* **526**, 1978–1990 (2018).
19. T. G. Beach *et al.*, Arizona Parkinson's Disease Consortium, Unified staging system for Lewy body disorders: Correlation with nigrostriatal degeneration, cognitive impairment and motor dysfunction. *Acta Neuropathol.* **117**, 613–634 (2009).
20. K. Obi *et al.*, Relationship of phosphorylated alpha-synuclein and tau accumulation to Aβeta deposition in the cerebral cortex of dementia with Lewy bodies. *Exp. Neurol.* **210**, 409–420 (2008).
21. D. G. Walker *et al.*, Arizona Parkinson Disease Consortium, Changes in properties of serine 129 phosphorylated alpha-synuclein with progression of Lewy-type histopathology in human brains. *Exp. Neurol.* **240**, 190–204 (2013).
22. M. Swirski *et al.*, Evaluating the relationship between amyloid-β and alpha-synuclein phosphorylated at Ser129 in dementia with Lewy bodies and Parkinson's disease. *Alzheimers Res. Ther.* **6**, 77 (2014).
23. S. Xu, P. Chan, Interaction between neuromelanin and alpha-synuclein in Parkinson's disease. *Biomolecules* **5**, 1122–1142 (2015).
24. K. E. Paleologou *et al.*, Phosphorylation at Ser-129 but not the phosphomimics S129E/D inhibits the fibrillation of alpha-synuclein. *J. Biol. Chem.* **283**, 16895–16905 (2008).
25. G. Fairfoul *et al.*, Alpha-synuclein RT-QuIC in the CSF of patients with alpha-synucleinopathies. *Ann. Clin. Transl. Neurol.* **3**, 812–818 (2016).
26. G. Rossetti *et al.*, Conformational ensemble of human alpha-synuclein physiological form predicted by molecular simulations. *Phys. Chem. Chem. Phys.* **18**, 5702–5706 (2016).
27. N. K. Majbour *et al.*, Oligomeric and phosphorylated alpha-synuclein as potential CSF biomarkers for Parkinson's disease. *Mol. Neurodegener.* **11**, 7 (2016).
28. V. N. Uversky, Protein folding revisited. A polypeptide chain at the folding-misfolding-nonfolding cross-roads: Which way to go? *Cell. Mol. Life Sci.* **60**, 1852–1871 (2003).
29. L. Pieri, K. Madiona, R. Melki, Structural and functional properties of prefibrillar alpha-synuclein oligomers. *Sci. Rep.* **6**, 24526 (2016).
30. A. L. Mahul-Mellier *et al.*, The process of Lewy body formation, rather than simply alpha-synuclein fibrillization, is one of the major drivers of neurodegeneration. *Proc. Natl. Acad. Sci. U.S.A.* **117**, 4971–4982 (2020).
31. M. F. Duffy *et al.*, Quality over quantity: Advantages of using alpha-synuclein preformed fibril triggered synucleinopathy to model idiopathic Parkinson's disease. *Front. Neurosci.* **12**, 621 (2018).
32. R. J. Karpowicz Jr., J. Q. Trojanowski, V. M. Lee, Transmission of alpha-synuclein seeds in neurodegenerative disease: Recent developments. *Lab. Invest.* **99**, 971–981 (2019).
33. S. Elfarash *et al.*, Organotypic slice culture model demonstrates inter-neuronal spreading of alpha-synuclein aggregates. *Acta Neuropathol. Commun.* **7**, 213 (2019).
34. M. Okochi *et al.*, Constitutive phosphorylation of the Parkinson's disease associated alpha-synuclein. *J. Biol. Chem.* **275**, 390–397 (2000).
35. A. Oueslati, Implication of alpha-synuclein phosphorylation at S129 in synucleinopathies: What have we learned in the last decade? *J. Parkinsons Dis.* **6**, 39–51 (2016).
36. S. Tenreiro, K. Eckeremann, T. F. Outeiro, Protein phosphorylation in neurodegeneration: Friend or foe? *Front. Mol. Neurosci.* **7**, 42 (2014).
37. K. Y. Chau, H. L. Ching, A. H. Schapira, J. M. Cooper, Relationship between alpha synuclein phosphorylation, proteasomal inhibition and cell death: Relevance to Parkinson's disease pathogenesis. *J. Neurochem.* **110**, 1005–1013 (2009).
38. V. Sancenon *et al.*, Suppression of alpha-synuclein toxicity and vesicle trafficking defects by phosphorylation at S129 in yeast depends on genetic context. *Hum. Mol. Genet.* **21**, 2432–2449 (2012).
39. T. Kuwahara, R. Tonegawa, G. Ito, S. Mitani, T. Iwatsubo, Phosphorylation of alpha-synuclein protein at Ser-129 reduces neuronal dysfunction by lowering its membrane binding property in *Caenorhabditis elegans*. *J. Biol. Chem.* **287**, 7098–7109 (2012).
40. M. R. Ma, Z. W. Hu, Y. F. Zhao, Y. X. Chen, Y. M. Li, Phosphorylation induces distinct alpha-synuclein strain formation. *Sci. Rep.* **6**, 37130 (2016).
41. B. A. Silva, L. Breydo, V. N. Uversky, Targeting the chameleon: A focused look at alpha-synuclein and its roles in neurodegeneration. *Mol. Neurobiol.* **47**, 446–459 (2013).
42. S. H. Shahmoradian *et al.*, Lewy pathology in Parkinson's disease consists of crowded organelles and lipid membranes. *Nat. Neurosci.* **22**, 1099–1109 (2019).
43. N. Landeck *et al.*, A novel multiplex assay for simultaneous quantification of total and S129 phosphorylated human alpha-synuclein. *Mol. Neurodegener.* **11**, 61 (2016).
44. N. N. Vaikath *et al.*, Heterogeneity in alpha-synuclein subtypes and their expression in cortical brain tissue lysates from Lewy body diseases and Alzheimer's disease. *Neuropathol. Appl. Neurobiol.* **45**, 597–608 (2019).
45. S. Di Giovanni *et al.*, Entacapone and tolcapone, two catechol O-methyltransferase inhibitors, block fibril formation of alpha-synuclein and beta-amyloid and protect against amyloid-induced toxicity. *J. Biol. Chem.* **285**, 14941–14954 (2010).
46. H. E. Kang, Y. Mo, R. Abd Rahim, H. M. Lee, C. Ryou, Prion diagnosis: Application of real-time quaking-induced conversion. *BioMed Res. Int.* **2017**, 5413936 (2017).
47. M. M. Dedmon, K. Lindorff-Larsen, J. Christodoulou, M. Vendruscolo, C. M. Dobson, Mapping long-range interactions in alpha-synuclein using spin-label NMR and ensemble molecular dynamics simulations. *J. Am. Chem. Soc.* **127**, 476–477 (2005).
48. V. Losasso, A. Pietropaolo, C. Zannoni, S. Gustinich, P. Carloni, Structural role of compensatory amino acid replacements in the alpha-synuclein protein. *Biochemistry* **50**, 6994–7001 (2011).
49. V. Hornak *et al.*, Comparison of multiple Amber force fields and development of improved protein backbone parameters. *Proteins* **65**, 712–725 (2006).
50. K. Lindorff-Larsen *et al.*, Improved side-chain torsion potentials for the Amber ff99SB protein force field. *Proteins* **78**, 1950–1958 (2010).
51. W. G. Hoover, Canonical dynamics: Equilibrium phase-space distributions. *Phys. Rev. A Gen. Phys.* **31**, 1695–1697 (1985).
52. L. Wang, R. A. Friesner, B. J. Berne, Replica exchange with solute scaling: A more efficient version of replica exchange with solute tempering (REST2). *J. Phys. Chem. B* **115**, 9431–9438 (2011).
53. T. Terakawa, T. Kameda, S. Takada, On easy implementation of a variant of the replica exchange with solute tempering in GROMACS. *J. Comput. Chem.* **32**, 1228–1234 (2011).
54. S. Neal, A. M. Nip, H. Zhang, D. S. Wishart, Rapid and accurate calculation of protein 1H, 13C and 15N chemical shifts. *J. Biomol. NMR* **26**, 215–240 (2003).
55. B. M. Bulheller, J. D. Hirst, DichroCalc—Circular and linear dichroism online. *Bioinformatics* **25**, 539–540 (2009).
56. J. R. Allison, R. C. Rivers, J. C. Christodoulou, M. Vendruscolo, C. M. Dobson, A relationship between the transient structure in the monomeric state and the aggregation propensities of alpha-synuclein and beta-synuclein. *Biochemistry* **53**, 7170–7183 (2014).
57. D. K. Wilkins *et al.*, Hydrodynamic radii of native and denatured proteins measured by pulse field gradient NMR techniques. *Biochemistry* **38**, 16424–16431 (1999).
58. M. T. Ardah *et al.*, Inhibition of alpha-synuclein seeded fibril formation and toxicity by herbal medicinal extracts. *BMC Complement. Med. Ther.* **20**, 73 (2020).
59. L. Stoppini, P. A. Buchs, D. Muller, A simple method for organotypic cultures of nervous tissue. *J. Neurosci. Methods* **37**, 173–182 (1991).
60. N. Gogolla, I. Galimberti, V. DePaola, P. Caroni, Staining protocol for organotypic hippocampal slice cultures. *Nat. Protoc.* **1**, 2452–2456 (2006).